Synthesis and interaction of unsaturated chemical probes with *Mycobacterium tuberculosis* CYP124A1

Luz Díaz-Storani[a,‡], Anaelle A. Clary[b,‡,#], Diego M. Moreno[a], María Sol Ballari[a], Exequiel O. J. Porta[a], Andrea B. J. Bracca[a], Jonathan B. Johnston[b,§,*], and Guillermo R. Labadie[a,*]

[a]*Instituto de Química Rosario (IQUIR-CONICET), Facultad de Ciencias Bioquímicas y Farmacéuticas, Universidad Nacional de Rosario. Suipacha 531, S2002LRK, Rosario, Argentina.*

[b]*Department of Pharmaceutical Chemistry, University of California, San Francisco, CA 94158-2517, United States.*

[‡]*These authors contributed equally to this work*

[§]*Current address: Pact Pharma, 2 Corporate Drive. South San Francisco, CA 94080.*

[#]*Current address: Institut de Recherche Servier, 11 rue des Moulineaux, 92210 Suresnes, France.*

**Corresponding authors*

E-mail: labadie@iquir-conicet.gov.ar, jb.johnst@gmail.com

Abstract

A series of C15–C20 isoprenyl derivatives bearing terminal alkenyl and alkynyl groups were synthesized as possible substrates of the methyl-branched lipid ω-hydroxylase CYP124A1 from *Mycobacterium tuberculosis*. The interactions of each compound with the enzyme active site were characterized using UV-vis spectroscopy. We found that the C10 and C15 analogs bind with an affinity similar to the corresponding parent C10 and C15 substrates geraniol and farnesol, respectively. Three analogs (C10-ω-ene, C10-ω-yne, C15-ω-yne) interact with the proximal side of the heme iron by coordinating to the oxygen atom of the ferric heme, as judged by the appearance of typical Type-IA binding spectra. On the other hand, the C15-ω-ene analog interacts with the ferric heme by displacing the bound water that generates a typical Type I binding spectrum. We were unable to detect P450-mediated oxidation of these probes following extended incubations with CYP124A1 in our reconstituted assay system, whereas a control reaction containing farnesol was converted to ω-hydroxy farnesol under the same conditions. To understand the lack of detectable oxidation, we explored the possibility that the analogs were acting as mechanism-based inhibitors, but we were unable to detect time-dependent loss of enzymatic activity. In order to gain insight into the lack of detectable turnover or time-dependent inhibition, we examined the interaction of each compound with the CYP124A1 active site using molecular docking simulations. The docking studies revealed a binding mode where the terminal unsaturated functional groups were sequestered within the methyl-binding pocket, rather than positioned close to the heme iron for oxidation. These results aid in the design of specific inhibitors of *Mtb*-CYP124A1, an interesting enzyme that is implicated in the oxidation of methyl-branched lipids, including cholesterol, within a deadly human pathogen.

Keywords: CYP124A1, Chemical Probes, Docking, Isoprenyl alcohol, *Mycobacterium tuberculosis*.

1. Introduction

Tuberculosis (TB) is an infectious pulmonary disease caused by the bacterium *Mycobacterium tuberculosis* (Mtb), and primarily afflicts the developing world. TB is a leading cause of global mortality and one of the top 10 causes of death. Individuals with compromised immune system are particularly vulnerable. In 2019, 10.0 million people developed TB around the world, and an estimated 1.4 million deaths were registered. Around 1.7 billion people may already have a latent TB infection and are at risk of developing active TB disease during their lifetime. Approximately 10% of those individuals with latent infections will shift to the active form of the disease, and one in six of them will die.[1]

There have been many encouraging developments in diagnosing and treating TB. As a result, the number of individuals infected with TB has markedly declined since 2005 and the total number of deaths fell to 1.4 million people in 2019.[1] Much of the success is due to improvements in diagnosing, monitoring, and treating the disease. Despite this progress, efforts to slow the spread of TB infection and eradicate the disease continue to be complicated by the evolution of virulent, drug-resistant Mtb strains.[2] The appearance of multidrug-resistant (MDR-TB) and extremely drug resistant TB (XDR-TB) strains has, in fact, led to the alarming identification of totally drug resistant (TDR-TB) strains.[3–5]

One of the most exciting recent developments in infectious disease research is the approval of bedaquiline in 2012, the first new drug approved for treating TB/MDR-TB in over 40 years. However, new treatments are urgently needed for children and better and shorter treatments for people living with HIV-TB. Therefore, there is an urgent need to identify and develop new drugs and new drug-targeting strategies to treat TB in both its latent and active forms.

The sequencing of the Mtb genome reported in 1998,[6] a major breakthrough in TB research, revealed that approximately 10% of its genes are involved in lipid biosynthesis and metabolism, consistent with the complex lipids produced and utilized by Mtb.[7,8] Surprisingly, twenty cytochrome P450 enzymes were among these lipid-related genes, at the time an unprecedented number in a bacterial genome.[9,10] The retention of these genes within a rapidly evolving organism suggests that

they play critical roles in the biochemistry of this pathogen. It is known that when Mtb is in the active phase of infection, it utilizes cholesterol as a carbon and energy source, and because of that, the CYP functionality and substrate promiscuity strongly suggest their involvement as a key factor for Mtb survival. Indeed, several P450 genes (CYP125A1, CYP121A1, and CYP128A1) are conditionally essential for Mtb viability while other Mtb CYP enzymes can be considered potential drug targets,[9–14] since they exhibit low sequence identity with human P450 isoforms.

CYP51, one of the twenty Mtb P450 enzymes, got its function assigned based on its sequence homology to known enzymes, whereas the remaining nineteen Mtb P450 enzymes represent new P450 families. CYP51 was the first Mtb P450 enzyme to be characterized and investigated as a platform for drug design.[15–17] The proximity and organization of genes sometimes provides a clue to the function of a target gene, especially in bacterial genomes.[18] CYP121, another Mtb P450 enzyme, was found by high-resolution structural characterization and biochemical studies to catalyze the formation of cyclodityrosine.[19–24] Structural and biophysical characterization of Mtb CYP130 revealed large domain movements associated with the binding of azole drugs,[25] and although a CYP130 clone proved to catalyze *N*-demethylation of dextromethorphan,[26] its native substrate and function remain unknown. CYP125 and CYP142, are involved in themultistep oxidation of the cholesterol side chain.[9,11,27–32] CYP141 is one of the Mtb P450 enzymes that are distributed only within the “Mtb Complex”, TB-causing strains that, in addition to Mtb, include *M. bovis*, *M. africanum* and *M. microti*.[9] Mtb CYP141A1 has been reported to be a sensitive diagnostic target for the detection of Mtb in sputum samples.[33] CYP144 has been biochemically and structurally characterized,[34,35] and although it was found that this enzyme shares binding similarities with CYP121,[36] its substrate and function remain unknown. CYP128A1 is postulated to activate the polyisoprenoid MK-9 (DH-2) for hydroxylation at the ω-position of the lipid chain.[37] This would allow for subsequent activation by 3'-phosphoadenosine-5'-phosphosulfate (PAPS) synthase and then sulfation by SFT3.

Mtb CYP124A1 is a lipid hydroxylase with a preference for the ω-position of methyl-branched lipids. This enzyme exhibits broad catalytic activity towards various lipid substrates, including sterols, fatty acids, and isoprenoid alcohols.[28,31,38] In the Mtb complex, CYP124A1 is situated next

to the three gene operon for CYP128A1 that includes an important sulfotransferase gene (*sft3*).[39] CYP124A1 participates in oxidation on lipid substrates (such as phytanic acid, farnesol, cholesterol, etc), producing an alcohol product, which can undergo additional rounds of oxidation to form the aldehyde and carboxylic acid, catalyzed by CYPs from the same family (i.e. CYP125 and CYP142). CYP124A1 also catalyzes less efficiently the epoxidation of alkenes.[31] Crystal and co-crystal structures were solved for the holo-enzyme as well as the phytanic acid-bound form.[38] The co-crystal structure suggests a model by which the CYP124A1 active site enforces unfavorable regioselectivity,[38,40] whereby a small cleft situated near the heme iron binds one of the methyl groups of the methyl-branched substrates, which positions the other methyl group near the heme iron where it can undergo oxidation. In the absence of methyl branching, the terminal end of linear lipid chains is thought to equilibrate between being bound in the methyl-binding pocket and being positioned near the heme iron. Regioselectivity appears to be substrate dependent, i.e., with fatty acids and fatty alcohols the remainder of the lipid chain interacts with the barrel of the CYP124A1 active site leading to the heme, however, with bulkier sterol substrates, the active site channel is too restrictive to allow full diffusion of the substrate all the way to the heme iron. On this last case, regioselectivity is enforced by clamping the steroid nucleus to the so-called “letterbox active site model”. It was observed that the substrate needs to have a certain scaffold that allows the enzyme to accommodate in different ways in the active site of the CYP450 enzyme complex. This effect was what led different substrates to have different selectivity towards the enzyme, and it turned out to be particularly interesting to study. Thus, CYP124A1 appears to be a hybrid of the CYP125A1 and CYP142A1 active sites, whereby only the unfavorable ω-oxidation products are observed with steroid substrates with side chains at a minimum length of C25.[31] When comparing unbranched fatty acids, such as palmitic and lauric acid, with their ω-methyl branched analogs, it becomes evident that the presence of methyl branching appears to contribute significantly to catalytic activity,[38] whereas with sterols possessing unbranched side chains the contributions of the methyl group are less clear.[31]

In the present work, we aim to deepen the insight on the CYP124 mode of action and substrate requirements. To do this, we designed and synthesized unsaturated chemical probes that mimic isoprenoid compounds, which could interact with the enzyme of interest.

2. Results and Discussion

2.1. Design and synthesis of alkenyl and alkynyl chemical probes.

Cytochrome P450 enzymes are present in anabolic and catabolic pathways, typically catalyzing the oxidation of a wide variety of substrates, including oxidation of hydrocarbons and heteroatoms, dealkylations, and dehydrogenations.[41] Alkynes and alkenes are valuable tools to probe the chemical mechanism of cytochrome P450 enzymes as these functionalities may undergo oxidation by those enzymes that can lead to irreversible inhibition. Following catalytic turnover by a P450 enzyme of these functional groups, typically either the heme or an amino-acid residue near the active site is alkylated.[42] Using the known substrate selectivity and regiospecificity of CYP124A1,[38] we designed a series of chemical probes bearing olefin and alkyne functional groups at the ω-terminus of C10 and C15 isoprenyl lipids (**Figure 1**).

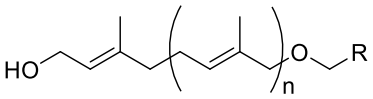

R= Vinyl, acetynyl n= 1,2

Figure 1. Designed chemical probes.

Four analogs have been designed and synthesized from commercially available isoprenols geraniol **1** and (*E,E*)-farnesol **8** (**Scheme 1**). In order to prepare compounds **5** and **7**, geraniol **1** was protected as the THP acetal **2** and oxidized on the terminal allylic position with SeO_2, *t*BuOOH and salicylic acid in DCM providing the alcohol **3**. Then, this intermediate was submitted to two different alkylating reactions with allyl bromide and propargyl bromide, in the presence of NaH as base in THF to obtain ethers **4** and **6**, respectively. Finally, THP acetals were deprotected with pyridinium p-toluenesulfonate (PPTS) providing the final probes **5** and **7** (**Scheme 1**).

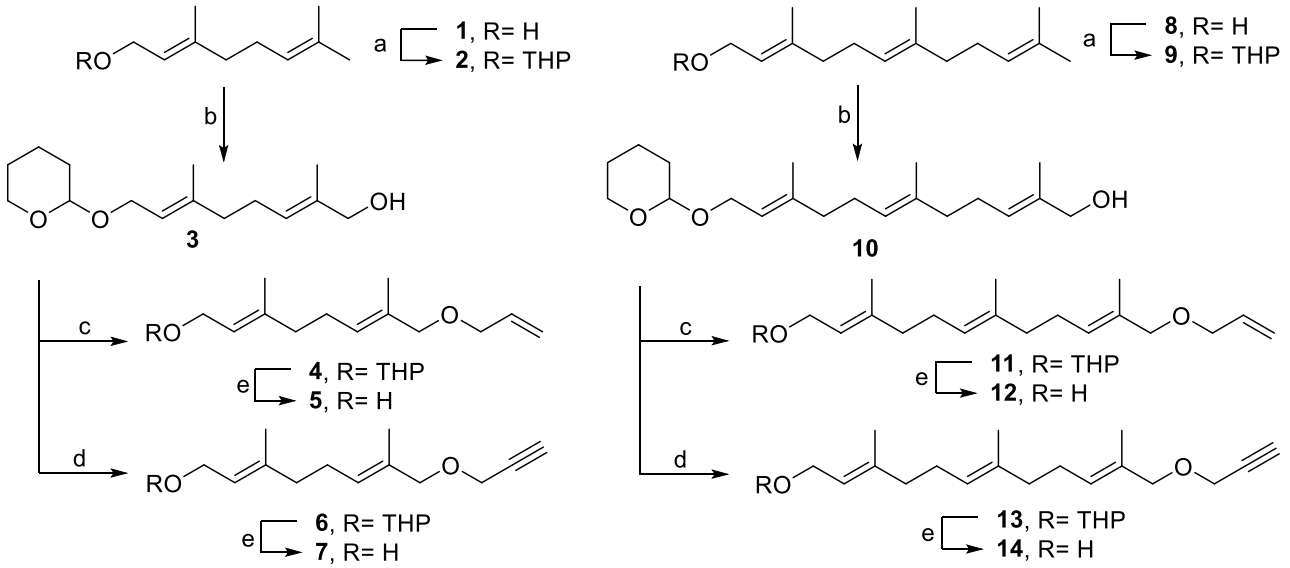

Scheme 1. Reagents and conditions: a) DHP, PPTS, DCM, rt, 6h, **2** (49 %), **9** (63 %); b) SeO_2, *t*-BuOOH, salicylic acid, DCM, rt, overnight, **3** (38 %), **10** (20 %); c) allyl bromide, NaH, THF, 0 °C to rt, overnight, **4** (50 %), **11** (40 %); d) propargyl bromide, NaH, THF, 0 °C to rt, overnight, **6** (49 %), **13** (52 %); e) PPTS, EtOH, reflux, 24h, **5** (54 %), **7** (91%), **12** (63 %), **14** (76 %).

Two additional analogs were synthesized from (*E,E*)-farnesol **8** (**Scheme 1**), following the same strategy presented above. (*E,E*)-farnesol **8** was protected with THP acetal giving **9**, which was subjected to the allylic oxidation generating a mixture of alcohols, being the primary alcohol **10** the main product. After separation and purification, alcohol **10** was converted on the allyl and propargyl ether under Williamson etherification conditions providing the expected terminal ethers **11** and **13**, respectively. Then, the final products **12** and **14** were obtained by hydrolysis of the THP acetals under mild acidic conditions (**Scheme 1**).

2.2. Interaction of unsaturated chemical probes with CYP124A1.

Following the synthesis of isoprenyl probes, we proceeded to evaluate them as CYP124A1 ligands. Absolute binding spectra informed on the interaction of ligands with the P450 active site. Representative absolute spectra are shown in **Figure 2** and indicate that the compounds bind specifically in the active site of CYP124A1 and displace the coordinated water molecule to generate the high-spin 5C form of the enzyme. This effect can be better appreciated in the UV-visible difference spectra shown in **Figure 3**. The nature and affinity of the interactions varied, producing both Type-I and Type-IA difference spectra. Specific ligand binding usually induces spectral changes due to the interaction of the ligand with the heme iron. Type-I binding spectra are characterized by a peak between 385 – 390 nm and a broad trough between 420 – 428 nm. These

signals increased in a concentration-dependent manner, generating a clean isosbestic point centered at 409 nm. Type-IA binding difference spectra generally show a broad peak centered at 406 nm and a trough at 425 – 430 nm.[31,42–46]

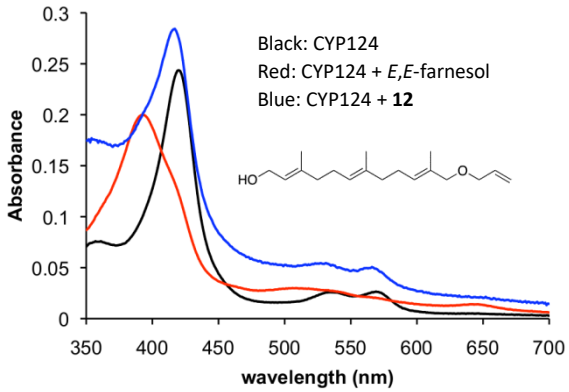

Figure 2. Spectra of CYP124 binding.

Type-I ligands are typically also substrates for P450 enzymes, and the absorbance changes indicate a shift from the low-spin 6-coordinated Fe^{3+} form of the enzyme, in which water is the sixth axial ligand, to a high-spin 5-coordinated Fe^{3+} form of the enzyme.[2] The magnitude of the absorbance change in the difference spectra reflects the percent conversion to the high-spin 5-coordinated enzyme form. In comparison with farnesol, which induces a nearly complete conversion to the high spin form of the enzyme at saturating concentrations,[38] the analogs tested here result in only a partial change. While farnesol was used as an isomers mixture in previous studies, in this work farnesyl ethers **12** and **14** were synthesized from (*E,E*)-farnesol, thus they preserved the (*E,E*) configuration.

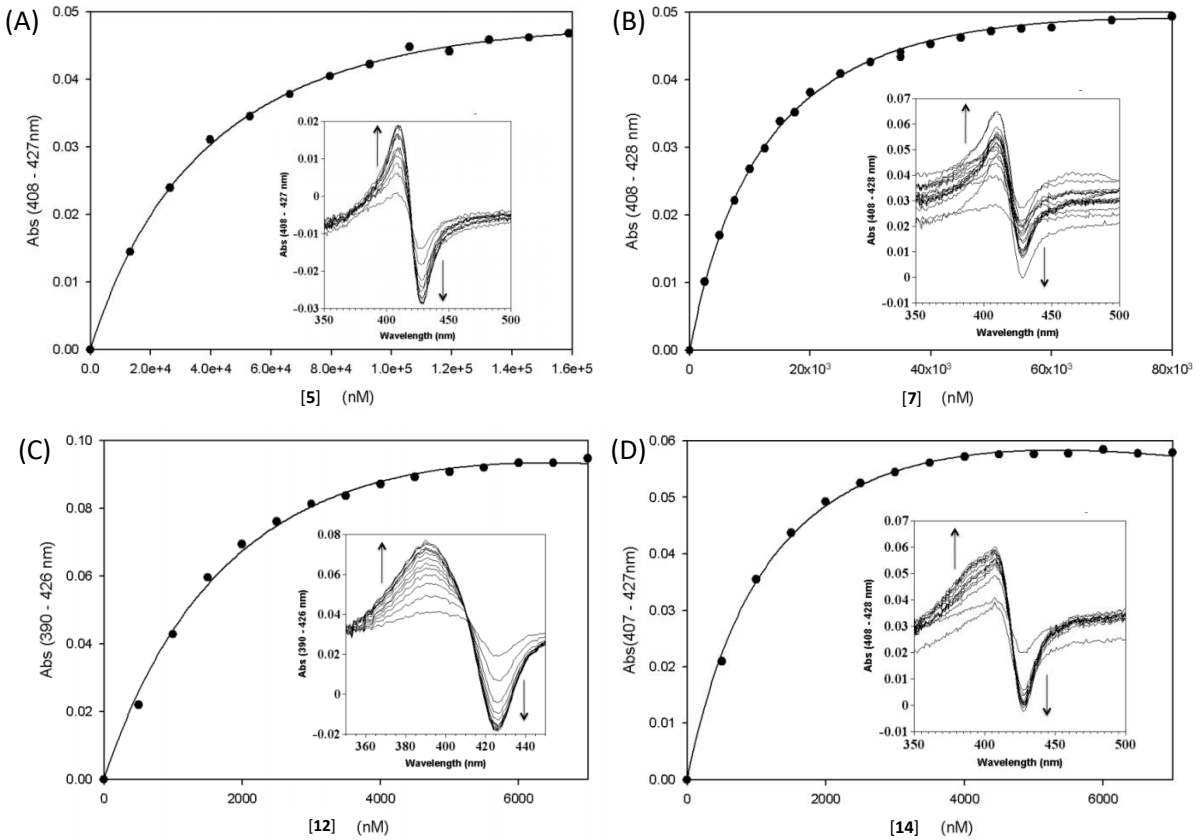

Figure 3. CYP124 UV-visible difference spectra and binding titration for compounds **5** (A), **7** (B), **12** (C) and **14** (D).

The apparent dissociation constant (Kd_{app}) values were determined by spectrophotometric binding titrations of CYP124A1 with each analog (**Figure 3**). The results are shown in **Table 1**. The Kd_{app} values exhibit a similar trend as we observed previously, *i.e.* more lipophilic analogs bind tighter within the active site.[38] A detailed look of the results revealed that the Kd_{app} differences observed between farnesol and geraniol are similar to their allyl and propargyl ethers, where the first binds 25 times more tightly to the enzyme, the farnesyl ethers are between 10 to 16.7 times better ligands than the geranyl analogs. Also, propargyl derivatives **7** and **14** are better ligands than their respective allylic analogs **5** and **12**, demonstrating that the restricted geometry and/or electron density of the distal carbon may be contributing to the binding.

Table 1. CYP124A1 dissociation constant

Analog	Kd_{app} (μM)	Binding
5	49.4 ± 4.6	Type-IA
7	14.6 ± 1.5	Type-IA
12	2.9 ± 0.4	Type-I
14	1.5 ± 0.1	Type-I/IA
Geraniol[38]	25.0 ± 1.8	Type-I
Farnesol[38]	1.04 ± 0.05	Type-I
Phytanic Acid[38]	0.220 ± 0.006	Type-I

Since the unsaturated probes appear to bind CYP124A1 and knowing that Type-I and Type-IA ligands can also be CYP substrates, we decided to determine if the compounds **5**, **7**, **12**, and **14** would be oxidized by CYP124A1. Catalytic assays were performed in which CYP124A1 was pre-incubated with saturating concentrations of each analog, and then spinach ferredoxin (Fdx) and spinach ferredoxin-$NADP^+$ reductase (Fdr), along with NADPH, were added to the reaction mixtures. However, no oxidation products were detected by GC-MS. Control reactions that incubated farnesol with CYP124A1 and the redox cofactor proteins showed the expected single terminal ω-hydroxy-farnesol product, as previously reported.[38] More information about these assays can be found in the Supporting Information. Furthermore, we tested if the ligands could inactivate the enzyme. It is known that reactive ligands are oxidized and subsequently converted to a species that is reactive towards the enzyme active site, being able to alkylate and destroy the catalytic activity of CYP124A1 in a time-dependent manner. We performed extended pre-incubations of each probe with enzyme, followed by dilution into fresh substrate and measured the residual activity. We were unable to detect a significant loss of enzyme activity over time after accounting for the background loss of catalytic activity.

Whereas CYP124A1 binds to geraniol **1** (C10) with an apparent affinity of 25.0 ± 1.8 μM, the C10 alkyne analog **7** bound on roughly the same order with an apparent dissociation constant value (Kd_{app}) of 14.6 ± 1.5 μM. Interestingly, the alkene analog **5** bound with decreased relative affinity of 49 ± 4.6 μM, likely reflecting the increased binding due to the more rigid terminal alkyne. Whereas geraniol binds in a clear Type-I manner, indicating that the water molecule was ejected from its axial coordination at the heme iron, the two C10 unsaturated analogs, compounds **5** and **7** bound as Type-IA ligands. This finding could show that they interact with the heme iron by coordination to the iron via the oxygen lone pair of the ether, or through the axial water ligand. Although geraniol was not detectably oxidized by CYP124A1, it also binds specifically and, in a manner, consistent with being a substrate. The two C10 analogs were not detectably oxidized by CYP124A1, consistent with our finding that these analogs bind in a Type-IA manner, whereby binding by coordination of oxygen to heme ironreduces the redox potential of the system relative to the water-liganded form, but to a lesser degree than typical nitrogenous ligands that coordinate to

the ferric heme iron. The C15 analogs **12** and **14** exhibited mixed behavior, whereas the substrate farnesol binds and is oxidized by the enzyme to the ω-hydroxy form, the two analogs were not detectably oxidized. The binding type exhibited was also different between the two C15 compounds. The alkyne derivative **14** bound as Type-IA meanwhile the alkene analog **12** bound as Type-I ligand. The differences in binding geometry likely reflect the different abilities of the terminal unsaturated portions of the molecule to sample different conformations, leading to different interactions with amino acid residues in the active site.

Molecules that tightly coordinate to the heme iron, such as azole compounds, can serve as potent inhibitors of P450 enzymes. Inhibition is complex, but it often takes place due to blocking of the active site by a tightly coordinated substrate analog. In our case, compared to isoprenols or methyl branched fatty acids, the interactions of the more electronegative ether oxygen reduce the redox potential of the heme iron by coordination, and it also makes reduction of the heme from ferric to the ferrous state more difficult. Moreover, binding is an equilibrium process, and one would expect that the opposite hydrocarbon end of the molecule could bind in an orientation that would position the unsaturated functional groups in proximity for catalysis. However, as no detectable oxidation products were observed, we hypothesized that the unsaturated carbon chain might be oriented in a way that it binds in the small cavity near the heme iron, similar as has been proposed for palmitic acid and other linear lipid chains.[38] In these cases, the flexible hydrocarbon chain leads to products ratio that reflect the stability during formation. However, only partial conversion of the low-spin to the high-spin form likely reflects the need for each substrate to bear alpha methyl-branching to the site of oxidation. In this model, the methyl branch closer to the alkyne or alkene functional groups would be near to the heme iron for oxidation, producing the oxidation of that carbon. The terminal alkyne and alkene are likely to bind the small lipophilic pocket adjacent to the heme iron rather than above the heme, preventing their oxidation, as have been reported for linear fatty acids. We performed molecular docking simulations in order to rationalize the interaction of the ligands with the CYP124A1 active site.

Starting with the CYP124A1 bound to phytanic acid crystallographic data (Protein Data Bank file: 2WM4), analogs **5**, **7**, **12**, and **14** were overlapped to this enzyme structure. Docking poses are

shown in **Figure 4**, where it can be appreciated that the probes share a similar conformation than phytanic acid in the original structure. Another representation are shown in **Figure 5**, where the active site limits are represented in grey. Long chain probes **12** and **14** accommodate following the phytanic acid pattern in the heme pocket, while for geranyl analogs **5** and **7** the alcohol takes a different conformation, causing the reduced bonding affinity previously observed (**Table 1**). It can also be appreciated that, for **5** and **7**, the probe interacts with the heme group by coordinating the ether oxygen, consistent with a Type-IA binding, which can be one of the factors involved in the lack of reaction for these ligands. For farnesyl analogs **12** and **14**, we could observe how the internal C from the allyl or propargyl group interact with the heme, leaving the branch pocket empty. The branch interaction, although weak, proved to be crucial for the enzyme to have oxidative activity.[38,47] The docking pose obtained for **12** is consistent with the Type-I binding experimentally determined.

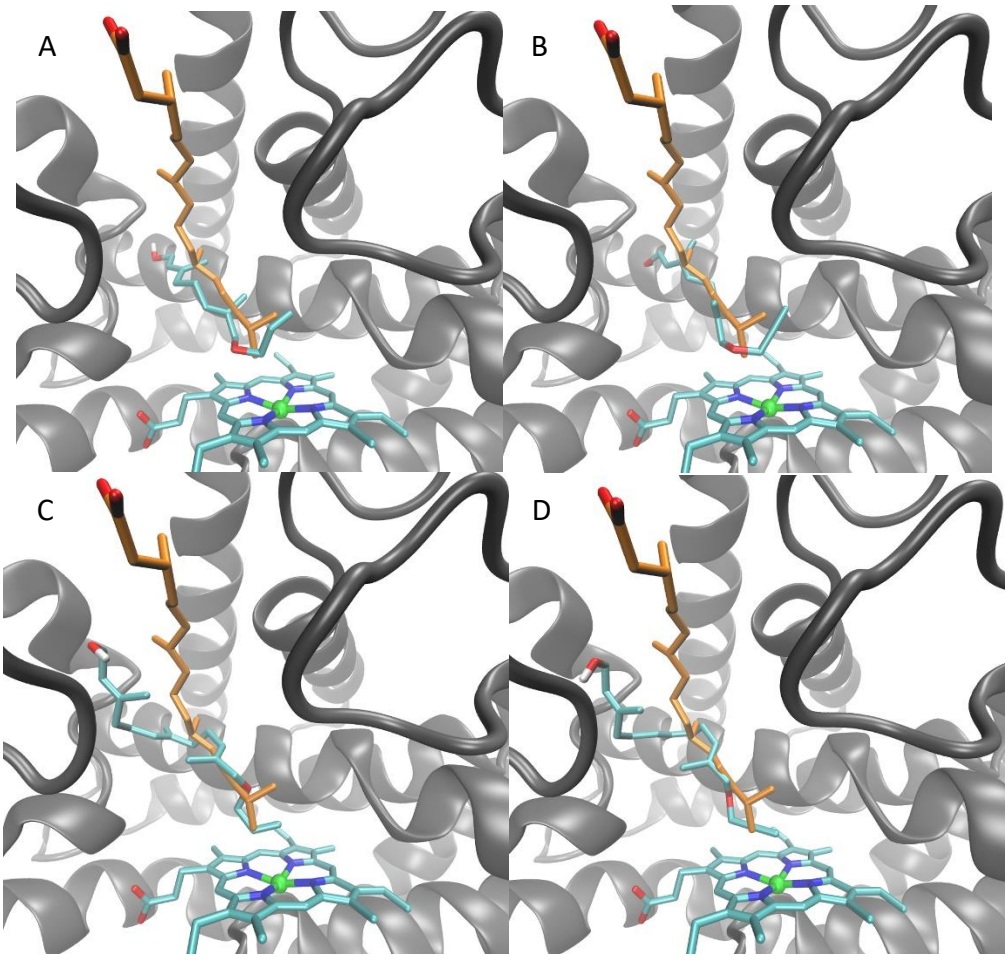

Figure 4. Overlay of the docking results with the CYP124-phytanic acid crystallographic structure (PDB code 2WM4). A) compound **5**, B) compound **7**, C) compound **12**, D) compound **14**. CYP124 protein are depicted in grey, C atoms from the heme group and the compounds are

shown in cyan, C atoms from phytanic acid in orange, O atoms in red, N atoms in blue, H atoms in white and Fe atom in green.

The data obtained from the second generation isoprenyl-based CYP124A1 inhibitors, along with the data obtained from the first generation steroidal-based inhibitors[31] should allow for deeper insight into the mechanism by which CYP124A1 binds and oxidizes various molecules. The steroidal nucleus seemed to be less connected with the binding and the catalytic activities, whereas chain length and extent of branching in that context seemed to be a better predictor of catalytic activity. In this regard, calibration of the chain length requirements was examined by the nor-series of cholesterol derivatives.[31] Even though the shortest chain analog, 24-bromochol-5-enol, was not detectably oxidized, it did exhibit an apparent spin shift in the heme state, indicating that compound does indeed bind in the catalytic cleft of the enzyme and competes with the normal substrate. For the steroidal substrates, the homologous Mtb P450 enzymes CYP125A1 and CYP142A1 exhibited a much higher catalytic activity than Mtb CYP124A1, but they also exhibited only ω-hydroxylation products, even though the chain could apparently reach far enough to oxidize interior carbon atoms. Thus, the letter box model restricts the chain from entering further into the active site and producing the ω-1 and ω-2 products that should be observed due to thermodynamic models of this process. With CYP124A1, on the other hand, the enzyme apparently can accommodate a larger variety of substrates by oxidizing methyl-branched lipids with apparent affinity but also showing a variety of major products that are present in higher yields. CYP124 probed to have a remarkable flexibility, which allows it to accommodate a wide variety of substrates, such as isoprenes, phytanic acid,[38] vitamin D,[48] steroids,[31,49] polyamines,[47] etc. Most of these compounds share the methyl branched chain, which will interact directly with the heme and undergo ω-oxidation. As was clear from all these studies, the variability of the assay conditions could have effect on the affinity or binding constant, and the ability to detect binding and subsequent oxidation. Nevertheless, we were able to determine that the isoprenyl analogs presented here(even though they are not substrates) had a high affinity for the enzyme active site, and could act as inhibitors. The function of Mtb CYP124 as a way to metabolize a prodrug has been described,[47] where the hydroxylated analog is presumably the active drug on a non-CYP target. The findings described in this work open doors to the design of a different type of anti-TB

drugs, which cannot be metabolized by CYP124, and which could act directly as its high affinity inhibitors for its active site.

3. Conclusion

Different probes were designed with reactive groups in the ω-position with the aim to study the mechanism of action of the Mtb CYP124 enzyme. We obtained new insights about a very interesting behavior of this enzyme with these chemical entities. We found that the Kd_{app} for those were similar to their analogous isoprenes, but no oxidation products were obtained. These results reaffirm that the branch side pocket plays an important role in CYP124A1 enzyme function. It is also evident that CYP124 prefers oxidation in inactivated sp^3 ω position over activated unsaturated carbon chain. These insights open up new possibilities for the design of new CYP124 inhibitors with high affinity for the heme that could displace the still unknown native substrate.

4. Materials and Methods

4.1. General Information.

All materials and reagents were of the highest grade commercially available and unless noted otherwise were obtained from Sigma-Aldrich (St. Louis, MO). Chemical reagents were purchased from commercial suppliers and used without further purification, unless otherwise noted. Solvents (hexanes, ethyl acetate, CH_2Cl_2, Et_2O) were distilled prior to use. CH_2Cl_2 was dried over P_2O_5. Reactions were monitored on pre-coated silica gel G or GP TLC plates. Spots were visualized under 254 nm UV light and/or by TLC staining. All reactions were performed under an atmosphere of nitrogen using oven-dried glassware and standard syringe/septa techniques. Column chromatography was performed with silica gel 60 (230-400 mesh). Yields were calculated for material judged homogeneous by thin layer chromatography (TLC) and nuclear magnetic resonance (^{1}H NMR).

^{1}H and ^{13}C NMR spectra were acquired on a Bruker Avance II 300 MHz (75.13 MHz) using $CDCl_3$ as solvent. Chemical shifts (δ) were reported in parts-per-million (ppm) downfield from tetramethylsilane as internal standard and coupling constants are in Hertz (Hz). Assignment of proton resonances was confirmed by correlated spectroscopy. High-resolution mass spectra (ESI-

HRMS) were recorded on a Bruker MicroTOF II with lock spray source. IR spectra were obtained using an FT-IR Shimadzu spectrometer and only partial spectral data are listed.

Synthesis of (*E*)-2-((3,7-dimethylocta-2,6-dien-1-yl)oxy)tetrahydro-2H-pyran (2).

To a solution of geraniol **1** (10.0 g; 64.9 mmol) in CH_2Cl_2 (50 mL) at 0 ºC, dihydropyran (DHP, 11,8 mL; 129,9 mmol) was added dropwise, followed by pyridinium *p*-toluenesulfonate (PPTS, 1,63 g; 6,5 mmol). After the reaction mixture was allowed to stir overnight at room temperature, it was partially evaporated, diluted with ethyl acetate and washed with $NaHCO_3$. The aqueous phase was extracted with ethyl acetate and the combined organic extracts were dried with Na_2SO_4 and concentrated under vacuum. After flash column chromatography, compound **2** was obtained as a colorless oil (7.50 g, 49 %). IR (film) υ 2924, 2870, 1668, 1024 cm^{-1}. ^1H NMR δ 5,35 (t, *J*= 6.8 Hz, 1H, 2-H); 5.09 (t, *J*= 6.2 Hz, 1H, 6-H); 4.62 (dd, *J*= 2.8 Hz and 4.1 Hz, 1H, 1'-H); 4.23 (dd, *J*= 6.3 Hz and 12.0 Hz, 1H, 1-H); 4.03 (dd, *J*= 7.5 Hz and 12.0 Hz, 1H, 1-H); 3.89 (m, 1H, 5'-H); 3.50 (m, 1H, 5'-H); 2.15-2.00 (m, 4H, 4-H, 5-H); 1.90-1.45 (m, 6H, 2'-H, 3'-H, 4'-H); 1.67* (s, 3H, 7-CH_3); 1.60* (s, 3H, 3-CH_3); 1.60*(s, 3H, 7-CH_3). ^{13}C NMR δ 140.2 (C), 131.6 (C), 124.0 (CH), 120.6 (CH), 97.8 (CH), 63.6 (CH_2), 62.3 (CH_2), 39.6 (CH_2), 30.7 (CH_2), 26.4 (CH_2), 25.6* (CH_3), 25.5* (CH_2), 19.6 (CH_2), 17.7 (CH_3), 16.4 (CH_3). HRMS calculated mass for $C_{15}H_{26}O_2Na$ $[M+Na]^+$ 261.1825, found m/z= 261.1823.

Synthesis of (2*E*,6*E*)-2,6-dimethyl-8-((tetrahydro-2H-pyran-2-yl)oxy)octa-2,6-dien-1-ol (3).

THP-geraniol **2** (7.5 g, 31.50 mmol) was dissolved in CH_2Cl_2 (40 mL) and treated with *t*-BuOOH (14 mL, 57.50 mmol), SeO_2 (350 mg, 3.20 mmol) and salicylic acid (440 mg, 3.20 mmol). The mixture was stirred overnight at room temperature. Then, the solvent was partially evaporated and *t*-BuOOH was eliminated by washing three times with toluene followed by evaporation. The residue was dissolved in diethyl ether and washed with saturated $NaHCO_3$. The organic extracts were washed with brine, dried with Na_2SO_4 and concentrated under vacuum. The crude extract was dissolved in methanol (50 mL), cooled at -10 ºC and treated with small portions of $NaBH_4$ (1.5 g, 38.1 mmol). The mixture was stirred at the same temperature for 2 h. After that period, the reaction was quenched with the addition of water (50 mL) at 0ºC. The methanol was evaporated and the aqueous phase was saturated with the addition of NaCl. After extraction with ether, the combined

organic extracts were dried with Na_2SO_4 and concentrated under vacuum. Purification by flash column chromatography generated 3.06 g of alcohol **3** (38 % yield) as a colorless oil. ^{1}H NMR δ 5.33 (q, *J*= 12.7 Hz, 2H, 2-H, 6-H); 4.59 (dd, *J*= 3.0 and 4.0 Hz, 1H, 1'-H); 4.20 (dd, *J*= 11.5 and 6.0 Hz, 1H, 1-H); 3.93 (s, 2H, 8-H); 3.89-3.79 (m, 1H, 5'-H); 3.53-3.42 (m, 1H, 5'-H); 2.15-2.00 (m, 4H, 4-H, 5-H); 1.64* (s, 3H, 3-CH_3); 1.62* (s, 3H, 7-CH_3); 1.90-1.45 (m, 6H, 2'-H, 3'-H, 4'-H).^{13}C NMR δ 139.7 (C), 135.1 (C), 125.4 (CH), 120.2 (CH), 97.8 (CH), 68.7 (CH_2), 63.6 (CH_2), 62.2 (CH_2), 39.1 (CH_2), 30.6* (CH_2), 25.7* (CH_2), 25.5* (CH_2), 19.5* (CH_2), 16.3* (CH_3), 13.6* (CH_3). HRMS calculated mass for $C_{15}H_{26}O_3Na$ $[M+Na]^+$ 277.1785, found m/z= 277.1785.

Synthesis of 2-(((2*E*,6*E*)-8-(allyloxy)-3,7-dimethylocta-2,6-dien-1-yl)oxy)tetrahydro-2H-pyran (4).

A solution of alcohol **3** (200.0 mg; 0.78 mmol) in THF (5 mL) was added to a suspension of NaH 42% (250.0 mg; 4.77 mmol) in THF (7 mL) at 0 ºC. The reaction mixture was stirred 1 h at 0 ºC followed by 2 h at room temperature. Then, allyl bromide was added (135 µL, 1.56 mmol) and the mixture was stirred another 24 h at room temperature. The reaction was quenched with saturated NH_4Cl and subjected to standard work-up. Purification by flash column chromatography gave 115 mg of ether **4** (50 % yield) as a colorless oil. IR (film) υ 2926, 2855, 1668,1076,1022 cm^{-1}. ^{1}H NMR δ 5,91 (ddt, *J*= 5.7, 10.3 and 17.2 Hz, 1H, -OCH_2CHCH_2); 5.38* (t, *J*=6.2Hz, 1H, 6-H); 5.35* (t, *J*= 6.2 Hz, 1H, 2-H); 5.26 (ddd, *J*= 1.6, 3.4 and 17.2 Hz, 1H, trans-OCH_2CHCH_2); 5.16 (ddd, *J*= 1.3, 3.0 and 10.3 Hz, 1H, cis-OCH_2CHCH_2); 4.62 (dd, *J*= 2.9 and 4.0 Hz, 1H, 1'-H); 4.23 (dd, *J*= 7.0 Hz and 12.0 Hz, 1H, 1-H); 4.20 (dd, *J*= 7.0 and 12.0 Hz, 1H, 1-H); 3.90 (dt, *J*=1.4 and 5.7 Hz, 2H, -OCH_2CHCH_2); 3.87 (m, 1H, 5'-H); 3.84 (s, 2H, 8-H); 3.50 (m, 1H, 5'-H); 2.16 (m, 2H, 5-H); 2.07 (m, 2H, 4-H); 1.68 (s, 3H, CH_3); 1.64 (s, 3H, CH_3); 1.45-1.90 (m, 6H, 2'-H, 3'-H, 4'-H). 13C NMR δ 139.6 (C), 135.0 (CH), 132.3 (C), 127.5 (CH), 120.9 (CH), 116.6 (CH_2), 97.7 (CH), 76.1 (CH_2), 70.3 (CH_2), 63.5 (CH_2), 62.1 (CH_2), 39.1 (CH_2), 30.7 (CH_2), 25.9 (CH_2), 25.5 (CH_2), 19.5 (CH_2), 16.3 (CH_3), 13.8 (CH_3). HRMS calculated mass for $[M+Na]^+$ $C_{18}H_{30}O_3Na$ 317.2087, found m/z= 317.2076.

Synthesis of (2*E*,6*E*)-8-(allyloxy)-3,7-dimethylocta-2,6-dien-1-ol (5).

A solution of **4** (86.0 mg; 0.29 mmol) in ethanol (3 mL) was treated with PPTS (7.7 mg; 0.03 mmol). The reaction mixture was stirred at reflux for 24 h. After that period, ethanol was evaporated, and the residue submitted to standard work-up procedure. Purification by flash column chromatography afforded 33 mg of alcohol **5** (54 % yield) as a colorless oil. IR (film) υ 3373, 2918, 2853, 1670, 1078, 922 cm^{-1}. ^{1}H NMR δ 5.91 (dd, *J*= 5.5 and 17.0 Hz, 1H, OCH_2CHCH_2); 5.40 (dd, *J*= 7.0 and 15.0 Hz, 2H, 2-H, 6-H); 5.26 (d, *J*= 17.2, 1H, OCH_2CHCH_2); 5.17 (d, *J*=10.3 Hz, 1H, OCH_2CHCH_2); 4.14 (d, *J*= 6.8 Hz, 2H, 1-H); 3.91 (d, J= 5.5 Hz, 2H, OCH_2CHCH2); 3.84 (s, 2H, 8-H); 2.16 (m, 2H, 5-H); 2.07 (m, 2H, 4-H); 1.68 (s, 3H, 7-CH_3); 1.65 (s, 3H, 3-CH_3). ^{13}C NMR δ 139.2 (C), 135.0 (CH), 132.5 (C), 127.5 (CH), 123.7 (CH), 116.8 (CH_2), 76.1 (CH_2), 70.5 (CH_2), 59.4 (CH_2), 39.1 (CH_2), 25.9 (CH_2), 16.2 (CH_3), 14.0 (CH_3). HRMS calculated mass for $C_{13}H_{22}O_2Na$ $[M+Na]^+$ 233.1517, found m/z= 233.1512.

Synthesis of 2-(((2*E*,6*E*)-3,7-dimethyl-8-(prop-2-yn-1-yloxy)octa-2,6-dien-1-yl)oxy)tetrahydro-2H-pyran (6).

According to the procedure described above for allyl ether **4**, a solution of alcohol **3** (200.0 mg; 0.78 mmol) in THF (5 mL) was added to a suspension of NaH 42% (230.6 mg; 4.03 mmol) in THF (7 mL) at 0 ^{o}C. After 3 h, allyl bromide was added (135 µL, 1.56 mmol) and the mixture was stirred 24 h at room temperature. The reaction was quenched with saturated NH_4Cl and subjected to standard work-up. Purification by flash column chromatography gave 112 mg of ether **6** (49 % yield) as a colorless oil. ^{1}H NMR δ 5.42* (t, *J*=6.8Hz, 1H, 2-H); 5.36* (t, *J*=7.4Hz, 1H, 6-H); 4.62 (dd, *J*= 3.2 and 3.9 Hz, 1H, 1'-H); 4.23 (dd, *J*= 5.8 and 11.9 Hz, 1H, 1-H); 4.01 (dd, *J*= 7.3 and 11.9 Hz, 1H, 1-H); 3.93 (s, 2H, 8-H); 3.87 (m, 1H, 5'-H); 3.50 (m, 1H, 5'-H); 2.40 (t, J= 2.4 Hz, 1H, -OCH_2CCH); 2.08 (m, 2H, 4-H); 1.67 (s, 3H, 7-CH_3); 1.64 (s, 3H, 3-CH_3); 1.45-1.90 (m, 6H, 2'-H, 3'-H, 4'-H). ^{13}C NMR δ 139.6 (C), 131.5 (C), 128.9 (CH), 121.0 (CH), 97.8 (CH), 80.0 (C), 75.7 (CH_2), 74.1 (CH), 63.6 (CH_2), 62.2 (CH_2), 56.3 (CH_2), 39.1 (CH_2), 30.7 (CH_2), 26.0 (CH_2), 25.5 (CH_2), 19.6 (CH_2), 16.3 (CH_3), 13.9 (CH_3). HRMS calculated mass for $C_{18}H_{28}O_3Na$ $[M+Na]^+$ 315.1931, found m/z= 315.1918.

Synthesis of (2*E*,6*E*)-3,7-dimethyl-8-(prop-2-yn-1-yloxy)octa-2,6-dien-1-ol (7).

The same procedure described above was followed for alcohol **5**. A solution of **6** (115.0 mg; 0.53mmol) in ethanol (6 mL) was treated with PPTS (29.0 mg; 0.11 mmol). After refluxing for 24 h, ethanol was evaporated, and the residue submitted to standard work-up procedure. Purification by flash column chromatography afforded 93.4 mg of alcohol **7** (91 % yield) as a colorless oil. IR (film) υ 3415, 3298, 2922, 2852, 1668, 1076 cm^{-1}. ^{1}H NMR δ 5.40 (m, 2H, 2-H, 6-H); 4.13 (d, J= 6.9 Hz, 2H, 1-H); 4.07 (d, J= 2.4 Hz, 2H, -OCH_2CCH); 3.92 (s, 2H, 8-H); 2.40 (t, *J*= 2.4 Hz, 1H, -OCH_2CCH); 2.17 (m, 2H, 5-H); 2.06 (m, 2H, 4-H); 1.67 (s, 3H, 7-CH_3); 1.64 (s, 3H, 3-CH_3). ^{13}C NMR δ 139.0 (C), 131.6 (C), 128.8 (CH), 123.8 (CH), 80.0 (C), 75.7 (CH_2), 74.2 (CH), 56.4 (CH_2), 59.3 (CH_2), 39.0 (CH_2), 25.9 (CH_2), 16.2 (CH_3), 13.9 (CH_3). HRMS calculated mass for $C_{13}H_{20}O_2$ Na $[M+Na]^+$ 231.1355, found m/z= 231.1347.

Synthesis of 2-(((2*E*,6*E*)-3,7,11-trimethyldodeca-2,6,10-trien-1-yl)oxy)tetrahydro-2H-pyran (9).

The same procedure as described above was used for synthesis of compound **2**. To a solution of farnesol **8** (2.0 g; 9.0 mmol), in CH_2Cl_2 (30 mL) at 0 ºC, DHP (1.64 mL; 18.0 mmol) was added dropwise, followed by PPTS (225.9 mg; 0.9 mmol). After standard work up including washing with $NaHCO_3$, purification by flash column chromatography afforded 1.73 g of compound **9** as a colorless oil (63 % yield). IR (film) υ 2939, 2872, 1668, 1022 cm^{-1}. ^{1}H NMR δ 5.35 (t, *J*= 6.8 Hz, 1H, 2-H); 5.08 (q, *J*= 6.4 Hz, 2H, 10-H, 6-H); 4.61 (dd, *J*= 2.9 and 3.9 Hz, 1H, 1'-H); 4.22 (dd, *J*= 6.4 and 11.9 Hz, 1H, 1-H); 4.01 (dd, *J*= 7.4 and 11.9 Hz, 1H, 1-H); 3.88 (m, 1H, 5'-H); 3.50 (m, 1H, 5'-H); 2.17-1.91 (m, 8H, 4-H, 5-H, 8-H, 9-H); 1.90-1.42 (m, 6H, 2'-H, 3'-H, 4'-H); 1.66* (s, 3H, 3-CH_3); 1.66* (s, 3H, 11-CH_3); 1.58* (s, 3H, 7-CH_3); 1.58* (s, 3H, 11-CH_3). ^{13}C NMR δ 140.2 (C), 135.2 (C), 131.2 (C), 124.3 (CH), 123.8 (CH), 120.6 (CH), 97.7 (CH), 63.6 (CH_2), 62.2 (CH_2), 39.7* (CH_2), 39.6* (CH_2), 30.7 (CH_2), 26.7* (CH_2), 26.3* (CH_2), 25.6* (CH_3), 25.5* (CH_2), 19.6 (CH_2), 17.6 (CH_3), 16.4* (CH_3), 16.0* (CH_3). HRMS calculated mass for $C_{20}H_{34}NaO_2$ $[M+Na]^+$ 329.2451, found m/z= 329.2438.

Synthesis of (2*E*,6*E*,10*E*)-2,6,10-trimethyl-12-((tetrahydro-2H-pyran-2-yl)oxy)dodeca-2,6,10-trien-1-ol (10).

THP-farnesol **9** (471 mg, 1.54 mmol) was dissolved in CH_2Cl_2 (9 mL) and treated with *t*-BuOOH (0.78 mL, 4.31 mmol), SeO_2 (17 mg, 0.15 mmol) and salicylic acid (21 mg, 0.15 mmol). The mixture was stirred at 10 ºC during 4 h. After that period, the solvent was partially evaporated and *t*-BuOOH was eliminated by repeating washings with toluene and evaporation. The residue was dissolved in ethyl acetate and washed with a saturated solution of $NaHCO_3$. The organic extract was dried with Na_2SO_4 and concentrated under vacuum. Primary alcohol **10** was obtained after purification by flash column chromatography (164.6 mg, 33 % yield) as a colorless oil. IR (film) υ 3445, 2924, 2854, 1022 cm^{-1}. ^1H NMR δ 5.36 (q, *J*= 7.6 Hz, 2H, 2-H, 10-H); 5.10 (t, *J*= 6.3 Hz, 1H, 6-H); 4.62 (dd, *J*= 2.9 and 4.0 Hz, 1H, 1'-H); 4.22 (dd, *J*= 6.2 and 11.9 Hz, 1H, 1-H); 4.02 (m, 1H, 1-H); 3.98 (s, 2H, 12-H); 3.88 (m, 1H, 5'-H); 3.50 (m, 1H, 5'-H); 2.30-1.95 (m, 8H, 4-H, 5-H, 8-H, 9-H); 1.90-1.45 (m, 6H, 2'-H, 3'-H, 4'-H); 1.67 (s, 3H, 11-CH_3); 1.65 (s, 3H, 3-CH_3); 1.59 (s, 3H, 7-CH_3).^{13}C NMR δ 140.1 (C), 134.8 (C), 134.7 (C), 125.8 (CH), 124.2 (CH), 120.7 (CH), 97.7 (CH), 68.9 (CH_2), 63.6 (CH_2), 62.3 (CH_2), 39.5 (CH_2), 39.2 (CH_2), 30.7 (CH_2), 26.2 (CH_2), 26.1 (CH_2), 25.5 (CH_2), 19.6 (CH_2), 16.4 (CH_3), 16.0 (CH_3), 13.7 (CH_3). HRMS calculated mass for $C_{20}H_{34}NaO_3$ $[M+Na]^+$ 345.2400, found m/z= 345.2396.

Synthesis of 2-(((2*E*,6*E*,10*E*)-12-(allyloxy)-3,7,11-trimethyldodeca-2,6,10-trien-1-yl)oxy)tetrahydro-2H-pyran (11).

As described for compound **4**, a solution of alcohol **10** (148.0 mg; 0.46 mmol) in THF (4 mL) was added to a suspension of NaH 42% (164.0 mg; 2.87 mmol) in THF (6 mL) at 0 ºC. After 3 h, allyl bromide was added (80 µL, 0.92mmol) and the mixture was stirred 24 h at room temperature. The reaction was quenched with saturated NH_4Cl and subjected to standard work-up. Purification by flash column chromatography afforded 67.3 mg of compound **11** (40 %) as a colorless oil. ^1H NMR δ 5.91 (ddt, *J*= 5.7, 10.5 Hz and 17.5 Hz, 1H, -OCH_2CHCH_2); 5.42-5.31 (m, 2H, 2-H, 10-H); 5.31-5.20 (m, 1H, -OCH_2CHCH_2 trans); 5.20-4.92 (m, 2H, 6-H, -OCH_2CHCH_2cis); 4.62 (d, *J*= 3.0 Hz, 1H, 1'-H); 4.23 (dd, *J*= 6.4 Hz and 11.8 Hz, 1H, 1-H); 4.02 (dd, *J*= 7.5 Hz and 12.0 Hz, 1H, C1-H); 3.90 (dt, *J*= 1.2 Hz and 5.7 Hz, 2H, -OCH_2CHCH_2); 3.89 (m, 1H, 5'-H); 3.84 (s, 2H, 12-H); 3.50 (m,

1H, 5'-H); 1.67 (s, 3H, 3-CH_3); 1.64 (s, 3H, 11-CH_3); 1.60 (s, 3H, 7-CH_3); 2.40-1.40 (m, 8H, 4-H, 5-H, 8-H, 9-H); 1.90-1.45 (m, 6H, 2'-H, 3'-H, 4'-H). ^{13}C NMR δ 140.2 (C), 135.0 (CH), 134.9 (C), 132.0 (C), 128.1 (CH), 124.2 (CH), 120.7 (CH), 116.7 (CH_2), 97.8 (CH), 76.2 (CH_2), 70.3 (CH_2), 63.6 (CH_2), 62.3 (CH_2), 39.6* (CH_2), 39.3* (CH_2), 30.7 (CH_2), 29.7 (CH_2), 26.3 (CH_2), 25.5 (CH_2), 19.6 (CH_2), 16.4* (CH_3), 16.0* (CH_3), 14.1 (CH_3). HRMS calculated mass for $C_{23}H_{38}O_3Na$ $[M+Na]^+$ 385.2713, found m/z= 385.2705.

Synthesis of (2*E*,6*E*,10*E*)-12-(allyloxy)-3,7,11-trimethyldodeca-2,6,10-trien-1-ol (12).

As previously described for alcohol **5**, a solution of **11** (67.3 mg; 0.13mmol) in ethanol (4 mL) was treated with PPTS (4.7 mg; 0.02 mmol). After refluxing for 24 h, ethanol was evaporated and the residue submitted to standard work-up procedure. Purification by flash column chromatography gave 22.2 mg of alcohol **12** (63 % yield) as a colorless oil. IR (film) υ 3387, 2922, 2855, 1670, 1078, 922 cm^{-1}. ^{1}H NMR δ 5.91 (ddt, *J*= 5.7, 10.4 and 17.2 Hz, 1H, -OCH_2CHCH_2); 5.41* (t, *J*= 7.0 Hz, 10-H); 5.38* (t, *J*= 7.9 Hz, 1H, 2-H); 5.26 (ddd, *J*= 1.6, 3.3 and 17.2 Hz, 1H, -OCH_2CHCH_2); 5.16 (ddd, *J*= 1.3, 3.0 and 10.3 Hz, 1H, -OCH_2CHCH_2); 5.08 (t, *J*= 8.6 Hz, 1H, 6-H); 4.14 (d, *J*= 6.9 Hz, 2H, 1-H); 3.90 (dt, *J*= 1.3 and 5.7 Hz, 2H, -OCH_2CHCH_2); 3.84 (s, 2H, 12-H); 1.95-2.25 (m, 8H, 4-H, 5-H; 8-H, 9-H); 1.67 (s, 3H, 11-CH_3); 1.64 (s, 3H, 3-CH_3); 1.60 (s, 3H, 7-CH_3). ^{13}C NMR δ 139.6 (C), 135.0 (CH), 132.0 (C), 128.0 (CH), 124.0 (CH), 123.4 (CH), 116.8 (CH_2), 76.2 (CH_2), 70.4 (CH_2), 59.4 (CH_2), 39.5 (CH_2), 39.2 (CH_2), 26.2 (CH_2), 16.3 (CH_3), 16.0 (CH_3), 13.9 (CH_3). HRMS calculated mass for $C_{18}H_{30}O_2Na$ $[M+Na]^+$ 301.2138, found m/z= 301.2136.

Synthesis of 2-(((2*E*,6*E*,10*E*)-3,7,11-trimethyl-12-(prop-2-yn-1-yloxy)dodeca-2,6,10-trien-1-yl)oxy)tetrahydro-2H-pyran (13).

As described for ether **4**, a solution of alcohol **10** (221.5 mg; 0.69 mmol) in THF (5 mL) was added to a suspension of NaH 42% (235.4 mg; 4.12 mmol) in THF (7 mL) at 0 ^oC. After 3 h, propargyl bromide was added (164 µL, 1.38mmol) and the mixture was stirred 24 h at room temperature. The reaction was quenched with saturated NH_4Cl and subjected to standard work-up. Purification by flash column chromatography afforded 130.7 mg of ether **13** (52 % yield) as a colorless oil. IR (film) υ 3417, 3304, 2941, 2874, 1076, 1026 cm^{-1}. ^{1}H NMR δ 5.41* (t, *J*= 6.8 Hz, 1H, 10-H); 5.35* (t, *J*= 6.9 Hz, 1H, 2-H); 5.11 (t, *J*= 6.1 Hz, 1H, 6-H); 4.62 (*J*= 2.9 Hz and 4.0 Hz, 1H, 1'-H); 4.23

(dd, *J*= 6.5 Hz and 12.0 Hz, 1H, 1-H); 4.06 (d, *J*=2.3 Hz, 2H, -OCH_2CCH); 3.99 (dd, *J*= 6.2 Hz and 13,6 Hz, 1H, 1-H); 3.92 (s, 2H, 12-H); 3.87 (m, 1H, 5'-H); 3.50 (m, 1H, 5'-H); 2.40 (t, *J*=2.4Hz, 1H, -OCH_2CCH); 1.95-2.25 (m, 8H, 4-H, 5-H, 8-H, 9-H); 1.67 (s, 3H, 11-H); 1.64 (s, 3H, 3-H); 1.59 (s, 3H, 7-CH_3); 1.45-1.90 (m, 6H, 2'-H, 3'-H, 4'-H). ^{13}C NMR δ 140.0 (C), 134.7 (C), 131.1 (C), 129.3 (CH), 124.2 (CH), 120.6 (CH), 97.7 (CH), 80.0 (C), 75.8 (CH_2), 74.0 (CH), 63.6 (CH_2), 62.2 (CH_2), 56.2 (CH_2), 39.5 (CH_2), 39.2 (CH_2), 30.7 (CH_2), 26.3 (CH_2), 26.2 (CH_2), 25.4 (CH_2), 19.6 (CH_2), 16.4 (CH_3), 15.9 (CH_3), 13.9 (CH_3). HRMS calculated mass for $C_{23}H_{36}O_3Na$ $[M+Na]^+$ 383.2557, found m/z= 383.2542.

Synthesis of (2*E*,6*E*,10*E*)-3,7,11-trimethyl-12-(prop-2-yn-1-yloxy)dodeca-2,6,10-trien-1-ol (14).

As described above for alcohol **5**, a solution of **13** (130.7 mg; 0.36mmol) in ethanol (6 mL) was treated with PPTS (9.1 mg; 0.04 mmol). After refluxing for 24 h, ethanol was evaporated and the residue submitted to standard work-up procedure. Purification by flash column chromatography afforded 72.1 mg of alcohol **14** (76 % yield) as a colorless oil. IR (film) υ 3416, 3304, 2922, 2853, 1668, 1074 cm^{-1}. ^{1}HNMR δ 5.34-5.45 (m, 2H, 2-H, 10-H); 5.09 (t, *J*= 6.3 Hz, 1H, 6-H); 4.12 (d, *J*= 6.9 Hz, 2H, 1-H); 4.05 (d, *J*= 2.4 Hz, 2H, -OCH_2CCH); 3.91 (s, 2H, 12-H); 2.40 (t, *J*=2.4 Hz, 1H, -OCH_2CCH); 2.95-1.95 (m, 8H, 4-H, 5-H, 8-H, 9-H); 1.66 (s, 3H, 11-CH_3); 1.63 (s, 3H, 3-CH_3); 1.58 (s, 3H, 7-CH_3).^{13}C NMR δ 139.6 (C), 134.9 (C), 131.2 (C), 129.3 (CH), 124.1 (CH), 123.4 (CH), 80.0 (C), 75.8 (CH_2), 74.1 (CH), 59.4 (CH_2), 56.3 (CH_2), 39.5 (CH_2), 39.2 (CH_2), 26.3 (CH_2), 26.3 (CH_2), 16.3 (CH_3), 16.0 (CH_3), 13.9 (CH_3). HRMS calculated mass for $C_{18}H_{28}O_2Na$ $[M+Na]^+$ 299.1981, found m/z= 299.1975.

4.2. Enzymes

The molecular cloning, over-expression, purification and general characterization of *M. tuberculosis* CYP124A1 was reported previously.[38] Ferredoxin (*Spinacia oleracea*), ferredoxin-$NADP^+$ reductase (*Spinacia oleracea*), catalase (Bovine), glucose-6-phosphate dehydrogenase (*Streptomyces sp*.) were obtained from Sigma-Aldrich.

4.3. UV-vis spectrophotometry

Absolute spectra were recorded on a dual-beam Cary UV-vis spectrophotometer as described previously using 1-cm path length quartz cuvettes.[38] Difference spectra were recorded as described previously[38] and the equilibrium binding affinity values and dissociation constants values were obtained from the concentration-dependent absorbance changes and fitted as described elsewhere.[28]

4.4. GC-MS analysis

GC-MS analyses were carried out using an Agilent 6850 gas chromatograph equipped with an HP-5MS column (30 m x 0.25 mm x 0.25 µm) and coupled to an Agilent 5973 Network MSD (Mass Selective Detector) in the electron ionization mode operating at -70 eV. Helium was used as the carrier gas at a flow rate of 1 mL/min. The temperature profile used to separate the compounds is as follows: hold at 70°C for 1 min, ramp by 10 °C per min up to 300 °C, and finally hold at 300 °C for 2.0 min. The inlet temperature was 250 °C and the detector temperature 230 °C. The flow from the injector was split with 1:10 going into the column for analysis.

4.5. Enzymatic evaluation of compounds

Cytochrome P450 CYP124A1 activity and product determinations assays were conducted by incubating 250 nM CYP124A1 with 50 µM – 250 µM compound, 5 µg catalase, 50 µg/mL ferredoxin, 0.16 U/mL ferredoxin-NADP+ reductase, 1 mM glucose-6-phosphate, 2.4 U/mL glucose-6-phosphate dehydrogenase, 5 mM $MgCl_2$, and 800 µM $NADP^+$ in 50 mM potassium phosphate pH 7.5 at 25 °C for 1 h. The reactions were quenched with an equal volume of 1 N HCl and extracted twice with TBME. The combined organic fractions were solubilized in BSTFA and dried under a stream of nitrogen gas. Derivatization was carried out for 30 min at 60 °C and the samples were then analyzed by GC-MS. Control reactions omitted either the CYP124A1 or the NADPH.

4.6. Time-dependent inhibition

Time-dependent inhibition of CYP124A1 by the unsaturated substrate analogs was assessed by pre-incubating 50 µM compound with 5 µM CYP124A1 in 50 mM potassium phosphate pH 7.5

containing ferredoxin, ferredoxin-$NADP^+$ reductase, catalase, and the NADPH-regenerating system, as described above. The control pre-incubation reactions were identical but instead contained only the buffer used to solubilize the substrate analogs. Over time, portions of the pre-incubated enzyme/inhibitor or enzyme/control reactions were diluted 1/20 into fresh buffer containing 50 μM of **5**, **7**, **12**, or **14**, spinach ferredoxin, ferredoxin-$NADP^+$ reductase and 1 mM NADPH and allowed to proceed for 10 min at 25 °C before quenching and analyzing by HPLC as described above. The residual activity percentages for each time point were calculated by taking the ratio of activity with **5**, **7**, **12**, or **14** remaining for the enzyme pre-incubated with analog vs. the control reaction and multiplying by 100.[31]

4.7. Molecular Docking Studies

Docking studies were carried out using Autodock 4.2 program.[50] Cytochrome P450 (CYP124) in complex with phytanic acid was used as the receptor protein and was obtained from Protein Data Bank (PDB entry = 2WM4). We eliminated *in-silico* the phytanic acid and prepared the receptor adding hydrogen atoms with AutoDockTools4.[50] We optimized in vacuum the structures of the four compounds at PBE/6-31G* level using Gaussian 09,[51] then the optimized structures of the ligands were prepared in pdbqt format using AutoDockTools4. The grid map was set to 70 × 70 × 70 points with a grid spacing of 0.375 Å centered on the iron ion of the heme group. We performed 256 docking simulations, then we selected the best protein-ligand structures.

Declaration of Competing Interest

The authors declare that they have no known competing financial interests or personal relationships that could have appeared to influence the work reported in this paper.

Acknowledgments

The authors wish to express their gratitude to UNR (Universidad Nacional de Rosario, Bio503), Agencia Nacional de Promoción Científica y Tecnológica (ANPCyT PICT- 2011-0589 awarded to GL) and CONICET (Consejo Nacional de Investigaciones Científicas y Técnicas, PIP 2012-14/0448). The authors also thank Professor Paul R. Ortiz de Montellano at UCSF for critical

reading of the manuscript and helpful suggestions. A.B.J.B., D.M. and G.R.L are members of the Research Career of the Consejo Nacional de Investigaciones Científicas y Técnicas of Argentina (CONICET). M.S.B, E.O.J.P. thanks CONICET for the award of a Fellowship. J.B.J. was supported by generous funding from the National Institute of Health (NIH AI074824 to Paul R. Ortiz de Montellano).

Notes

The authors declare no competing financial interest.

Appendix A. Supplementary data

Supplementary data to this article can be found online at https://doi.org/

References

1. World Health Organization. *Global Tuberculosis Report 2019*.; 2019.

2. Cole ST, Riccardi G. New tuberculosis drugs on the horizon. *Curr Opin Microbiol*. 2011;14(5):570-576. doi:10.1016/j.mib.2011.07.022

3. Migliori GB, De Iaco G, Besozzi G, Centis R, Cirillo DM. First tuberculosis cases in Italy resistant to all tested drugs. *Euro Surveill*. 2007;12(5):20-22. doi:10.2807/esw.12.20.03194-en

4. Velayati AA, Masjedi MR, Farnia P, et al. Emergence of new forms of totally drug-resistant tuberculosis bacilli: Super extensively drug-resistant tuberculosis or totally drug-resistant strains in Iran. *Chest*. 2009;136(2):420-425. doi:10.1378/chest.08-2427

5. Udwadia ZF, Amale RA, Ajbani KK, Rodrigues C. Totally Drug-Resistant Tuberculosis in India. *Clin Infect Dis*. 2012;54:579-581. doi:10.1093/cid/cir889

6. Cole ST, Brosch R, Parkhill J, et al. Deciphering thebiology of Mycobacterium tuberculosis from the complete genome sequence. *Nature*. 1998;393:537-544. doi:10.1038/29241

7. Brennan PJ. Structure, function, and biogenesis of the cell wall of Mycobacterium

tuberculosis. *Tuberculosis*. 2003;83(1-3):91-97. doi:10.1016/S1472-9792(02)00089-6

8. Minnikin DE, Kremer L, Dover LG, Besra GS. The Methyl-Branched Fortifications of Mycobacterium tuberculosis. *Chem Biol*. 2002;9:545-553. doi:10.1016/S1074-5521(02)00142-4

9. Ouellet H, Johnston JB, Ortiz de Montellano PR. The Mycobacterium tuberculosis cytochrome P450 system. *Arch Biochem Biophys*. 2010;493(1):82-95. doi:10.1016/j.abb.2009.07.011

10. McLean KJ, Clift D, Lewis DG, et al. The preponderance of P450s in the Mycobacterium tuberculosis genome. *Trends Microbiol*. 2006;14(5):220-228. doi:10.1016/j.tim.2006.03.002

11. Ouellet H, Johnston JB, Montellano PRO de. Cholesterol catabolism as a therapeutic target in Mycobacterium tuberculosis. *Trends Microbiol*. 2011;19(11):530-539. doi:10.1016/j.tim.2011.07.009

12. Agüero F, Al-Lazikani B, Aslett M, et al. Genomic-scale prioritization of drug targets: The TDR Targets database. *Nat Rev Drug Discov*. 2008;7(11):900-907. doi:10.1038/nrd2684

13. McLean KJ, Dunford AJ, Neeli R, Driscoll MD, Munro AW. Structure, function and drug targeting in Mycobacterium tuberculosis cytochrome P450 systems. *Arch Biochem Biophys*. 2007;464(2):228-240. doi:10.1016/j.abb.2007.03.026

14. Munro AW, McLean KJ, Marshall KR, et al. Cytochromes P450: Novel drug targets in the war against multidrug-resistant Mycobacterium tuberculosis. *Biochem Soc Trans*. 2003;31(3):625-630. doi:10.1042/BST0310625

15. Chen CK, Doyle PS, Yermalitskaya L V., et al. Trypanosoma cruzi CYP51 inhibitor derived from a Mycobacterium tuberculosis screen hit. *PLoS Negl Trop Dis*. 2009;3(2):3-12. doi:10.1371/journal.pntd.0000372

16. Podust LM, Poulos TL, Waterman MR. Crystal structure of cytochrome P450 14α-sterol demethylase (CYP51) from Mycobacterium tuberculosis in complex with azole inhibitors. *Proc Natl Acad Sci U S A*. 2001;98(6):3068-3073. doi:10.1073/pnas.061562898

595 17. Bellamine A, Mangla AT, Nes WD, Waterman MR. Characterization and catalytic properties
596 of the sterol 14α-demethylase from Mycobacterium tuberculosis. *Proc Natl Acad Sci U S A*.
597 1999;96(16):8937-8942. doi:10.1073/pnas.96.16.8937

598 18. Lamb DC, Guengerich FP, Kelly SL, Waterman MR. Exploiting Streptomyces coelicolor
599 A3(2) P450s as a model for application in drug discovery. *Structure*. 2006;3(2):27-40.
600 doi:10.1517/17425255.2.1.27

601 19. Belin P, Du MH Le, Fielding A, et al. Identification and structural basis of the reaction
602 catalyzed by CYP121, an essential cytochrome P450 in Mycobacterium tuberculosis. *Proc*
603 *Natl Acad Sci U S A*. 2009;106(18):7426-7431. doi:10.1073/pnas.0812191106

604 20. McLean KJ, Carroll P, Lewis DG, et al. Characterization of active site structure in CYP121:
605 A cytochrome P450 essential for viability of mycobacterium tuberculosis H37Rv. *J Biol*
606 *Chem*. 2008;283(48):33406-33416. doi:10.1074/jbc.M802115200

607 21. Dunford AJ, McLean KJ, Sabri M, et al. Rapid P450 heme iron reduction by laser
608 photoexcitation of Mycobacterium tuberculosis CYP121 and CYP51B1: Analysis of CO
609 complexation reactions and reversibility of the P450/P420 equilibrium. *J Biol Chem*.
610 2007;282(34):24816-24824. doi:10.1074/jbc.M702958200

611 22. Seward HE, Roujeinikova A, McLean KJ, Munro AW, Leys D. Crystal structure of the
612 Mycobacterium tuberculosis P450 CYP121-fluconazole complex reveals new azole drug-
613 P450 binding mode. *J Biol Chem*. 2006;281(51):39437-39443. doi:10.1074/jbc.M607665200

614 23. Leys D, Mowat CG, McLean KJ, et al. Atomic structure of Mycobacterium tuberculosis
615 CYP121 to 1.06 Å reveals novel features of cytochrome P450. *J Biol Chem*.
616 2003;278(7):5141-5147. doi:10.1074/jbc.M209928200

617 24. McLean KJ, Cheesman MR, Rivers SL, et al. Expression, purification and spectroscopic
618 characterization of the cytochrome P450 CYP121 from Mycobacterium tuberculosis. *J Inorg*
619 *Biochem*. 2002;91(4):527-541. doi:10.1016/S0162-0134(02)00479-8

620 25. Ouellet H, Podust LM, Ortiz De Montellano PR. Mycobacterium tuberculosis CYP130:

621 Crystal structure, biophysical characterization, and interactions with antifungal azole drugs.
622 *J Biol Chem*. 2008;283(8):5069-5080. doi:10.1074/jbc.M708734200

623 26. Ortega Ugalde S, Luirink RA, Geerke DP, Vermeulen NPE, Bitter W, Commandeur JNM.
624 Engineering a self-sufficient Mycobacterium tuberculosis CYP130 by gene fusion with the
625 reductase-domain of CYP102A1 from Bacillus megaterium. *J Inorg Biochem*.
626 2018;180(November 2017):47-53. doi:10.1016/j.jinorgbio.2017.12.003

627 27. Ouellet H, Guan S, Johnston JB, et al. Mycobacterium tuberculosis CYP125A1, a steroid
628 C27 monooxygenase that detoxifies intracellularly generated cholest-4-en-3-one. *Mol*
629 *Microbiol*. 2010;77(3):730-742. doi:10.1111/j.1365-2958.2010.07243.x

630 28. Johnston JB, Ouellet H, Ortiz De Montellano PR. Functional redundancy of steroid C26-
631 monooxygenase activity in Mycobacterium tuberculosis revealed by biochemical and genetic
632 analyses. *J Biol Chem*. 2010;285(47):36352-36360. doi:10.1074/jbc.M110.161117

633 29. Driscoll MD, McLean KJ, Levy C, et al. Structural and biochemical characterization of
634 Mycobacterium tuberculosis CYP142: Evidence for multiple cholesterol 27-hydroxylase
635 activities in a human pathogen. *J Biol Chem*. 2010;285(49):38270-38282.
636 doi:10.1074/jbc.M110.164293

637 30. Rosłoniec KZ, Wilbrink MH, Capyk JK, et al. Cytochrome P450 125 (CYP125) catalyses
638 C26-hydroxylation to initiate sterol side-chain degradation in Rhodococcus jostii RHA1. *Mol*
639 *Microbiol*. 2009;74(5):1031-1043. doi:10.1111/j.1365-2958.2009.06915.x

640 31. Johnston JB, Singh AA, Clary AA, et al. Substrate analog studies of the ω-regiospecificity of
641 Mycobacterium tuberculosis cholesterol metabolizing cytochrome P450 enzymes
642 CYP124A1, CYP125A1 and CYP142A1. *Bioorganic Med Chem*. 2012;20(13):4064-4081.
643 doi:10.1016/j.bmc.2012.05.003

644 32. McLean KJ, Lafite P, Levy C, et al. The structure of Mycobacterium tuberculosis CYP125:
645 Molecular basis for cholesterol binding in a P450 needed for host infection. *J Biol Chem*.
646 2009;284(51):35524-35533. doi:10.1074/jbc.M109.032706

33. Darban-Sarokhalil D, Fooladi AAI, Bameri Z, Nasiri MJ, Feizabadi MM. Cytochrome CYP141: A new target for direct detection of Mycobacterium tuberculosis from clinical specimens. *Acta Microbiol Immunol Hung*. 2011;58(3):211-217. doi:10.1556/AMicr.58.2011.3.4

34. Driscoll MD, McLean KJ, Cheesman MR, et al. Expression and characterization of Mycobacterium tuberculosis CYP144: Common themes and lessons learned in the M. tuberculosis P450 enzyme family. *Biochim Biophys Acta - Proteins Proteomics*. 2011;1814(1):76-87. doi:10.1016/j.bbapap.2010.05.015

35. Chenge J, Kavanagh ME, Driscoll MD, et al. Structural characterization of CYP144A1-a cytochrome P450 enzyme expressed from alternative transcripts in Mycobacterium tuberculosis. *Sci Rep*. 2016;6(May):1-12. doi:10.1038/srep26628

36. Kavanagh ME, Chenge J, Zoufir A, et al. A Fragment Profiling Approach to Inhibitors of the Orphan M. tuberculosis P450 CYP144A1. *Biochemistry*. 2017;56(11):1559-1572. doi:10.1021/acs.biochem.6b00954

37. Holsclaw CM, Sogi KM, Gilmore SA, et al. Structural characterization of a novel sulfated menaquinone produced by stf3 from Mycobacterium tuberculosis. *ACS Chem Biol*. 2008;3(10):619-624. doi:10.1021/cb800145r

38. Johnston JB, Kells PM, Podust LM, Ortiz De Montellano PR. Biochemical and structural characterization of CYP124: A methyl-branched lipid ω-hydroxylase from Mycobacterium tuberculosis. *Proc Natl Acad Sci U S A*. 2009;106(49):20687-20692. doi:10.1073/pnas.0907398106

39. Ngcobo NS, Chiliza ZE, Chen W, et al. Comparative Analysis, Structural Insights, and Substrate/Drug Interaction of CYP128A1 in Mycobacterium tuberculosis. *Int J Mol Sci*. 2020;21:4816. doi:10.3390/ijms21144816

40. Johnston JB, Ouellet H, Podust LM, Ortiz De Montellano PR. Structural control of cytochrome P450-catalyzed ω-hydroxylation. *Arch Biochem Biophys*. 2011;507(1):86-94. doi:10.1016/j.abb.2010.08.011

674 41. Ortiz de Montellano PR. Hydrocarbon Hydroxylation by Cytochrome P450 Enzymes. *Chem*
675 *Rev*. 2010;110:932-948. doi:10.1021/cr9002193

676 42. Ortiz de Montellano PR, ed. *Cytochrome P450: Structure, Mechanism, and Biochemistry,*
677 *Fourth Edition*. Springer International Publishing; 2015. doi:10.1007/978-3-319-12108-6

678 43. Schenkman OB, Cinti DL, Orrenius S, Moldeus P, Kraschnitz R. The Nature of the Reverse
679 Type I (Modified Type II) Spectral Change in Liver Microsomes. *Biochemistry*.
680 1972;11(23):4243-4251. doi:10.1021/bi00773a008

681 44. Kumaki K, Sato M, Kon H, Nebert DW. Correlation of type I, type II, and reverse type I
682 difference spectra with absolute changes in spin state of hepatic microsomal cytochrome P-
683 450 iron from five mammalian species. *J Biol Chem*. 1978;253(4):1048-1058.
684 doi:10.1016/s0021-9258(17)38109-7

685 45. Shimada T, Tanaka K, Takenaka S, et al. Reverse type I binding spectra of human
686 cytochrome P450 1B1 induced by flavonoid, stilbene, pyrene, naphthalene, phenanthrene,
687 and biphenyl derivatives that inhibit catalytic activity: A structure-function relationship study.
688 *Chem Res Toxicol*. 2009;22(7):1325-1333. doi:10.1021/tx900127s

689 46. Ouellet H, Kells PM, Ortiz De Montellano PR, Podust LM. Reverse type I inhibitor of
690 Mycobacterium tuberculosis CYP125A1. *Bioorganic Med Chem Lett*. 2011;21(1):332-337.
691 doi:10.1016/j.bmcl.2010.11.007

692 47. Bukhdruker S, Varaksa T, Grabovec I, et al. Hydroxylation of antitubercular drug candidate,
693 SQ109, by mycobacterial cytochrome p450. *Int J Mol Sci*. 2020;21(20):1-15.
694 doi:10.3390/ijms21207683

695 48. Vasilevskaya A V., Yantsevich A V., Sergeev G V., Lemish AP, Usanov SA, Gilep AA.
696 Identification of Mycobacterium tuberculosis enzyme involved in vitamin D and 7-
697 dehydrocholesterol metabolism. *J Steroid Biochem Mol Biol*. 2017;169:202-209.
698 doi:10.1016/j.jsbmb.2016.05.021

699 49. Varaksa T, Bukhdruker S, Grabovec I, et al. Metabolic fate of human immunoactive sterols

in Mycobacterium tuberculosis. *BioRxiv*. Published online 2020:2020.07.07.192294. doi:10.1101/2020.07.07.192294

50. Morris GM, Huey R, Lindstrom W, et al. AutoDock4 and AutoDockTools4: Automated Docking with Selective Receptor Flexibility. *J Comput Chem*. 2009;30(16):2785-2791. doi:10.1002/jcc.21256

51. Frisch MJ, Trucks GW, Schlegel HB, et al. Gaussian 09. Published online 2016.